



# CHORUS

This is the accepted manuscript made available via CHORUS. The article has been published as:

## Observation of Magnetoelectric Multiferroicity in a Cubic Perovskite System: $\text{LaMn}_3\text{Cr}_4\text{O}_{12}$

Xiao Wang, Yisheng Chai, Long Zhou, Huibo Cao, Clarina-dela Cruz, Junye Yang, Jianhong Dai, Yunyu Yin, Zhen Yuan, Sijia Zhang, Runze Yu, Masaki Azuma, Yuichi Shimakawa, Huimin Zhang, Shuai Dong, Young Sun, Changqing Jin, and Youwen Long

Phys. Rev. Lett. **115**, 087601 — Published 18 August 2015

DOI: [10.1103/PhysRevLett.115.087601](https://doi.org/10.1103/PhysRevLett.115.087601)

# Observation of Magnetoelectric Multiferroicity in a Cubic Perovskite System $\text{LaMn}_3\text{Cr}_4\text{O}_{12}$

Xiao Wang,<sup>1,2</sup> Yisheng Chai,<sup>1</sup> Long Zhou,<sup>1</sup> Huibo Cao,<sup>3</sup> Clarina-dela Cruz,<sup>3</sup> Junye Yang,<sup>1</sup> Jianhong Dai,<sup>1</sup> Yunyu Yin,<sup>1</sup> Zhen Yuan,<sup>1</sup> Sijia Zhang,<sup>1</sup> Runze Yu,<sup>4</sup> Masaki Azuma,<sup>4</sup> Yuichi Shimakawa,<sup>5</sup> Huimin Zhang,<sup>6</sup> Shuai Dong,<sup>6</sup> Young Sun,<sup>1,\*</sup> Changqing Jin,<sup>1,2</sup> and Youwen Long<sup>1,2,\*</sup>

<sup>1</sup>*Beijing National Laboratory for Condensed Matter Physics, Institute of Physics, Chinese Academy of Sciences, Beijing 100190, China*

<sup>2</sup>*Collaborative Innovation Center of Quantum Matter, Beijing 100190, China*

<sup>3</sup>*Quantum Condensed Matter Division, Neutron Scattering Science Directorate, Oak Ridge National Laboratory, Oak Ridge, Tennessee 37831, USA*

<sup>4</sup>*Materials and Structures Laboratory, Tokyo Institute of Technology, 4259 Nagatsuta, Midori-ku, Yokohama 226-8503, Japan*

<sup>5</sup>*Institute for Chemical Research, Kyoto University, Uji, Kyoto 611-0011, Japan*

<sup>6</sup>*Department of Physics, Southeast University, Nanjing 211189, China*

\*Corresponding E-mail: [ywlong@iphy.ac.cn](mailto:ywlong@iphy.ac.cn); [youngsun@iphy.ac.cn](mailto:youngsun@iphy.ac.cn)

PACS numbers: 75.50.-y, 77.84.-s, 81.40.Vw, 75.80.+q

## **Abstract**

The magnetoelectric multiferroicity is not expected to occur in a cubic perovskite system due to the high structural symmetry. By versatile measurements in magnetization, dielectric constant, electric polarization, neutron and X-ray diffraction, Raman scattering as well as theoretical calculations, we reveal that the A-site ordered perovskite  $\text{LaMn}_3\text{Cr}_4\text{O}_{12}$  with cubic symmetry is a novel spin-driven multiferroic system with strong magnetoelectric coupling effects. When magnetic field is applied in parallel/perpendicular to electric field, the ferroelectric polarization can be enhanced/suppressed significantly. The unique multiferroic phenomenon observed in this cubic perovskite cannot be understood by conventional spin-driven microscopic mechanisms. Instead, a nontrivial effect involving the interactions between two magnetic sublattices is likely to play a crucial role.

The magnetoelectric (ME) multiferroicity with coupled ferroelectric and magnetic orders have received much attention due to their great potential for numerous applications [1-8]. Perovskite is one of the most important material systems for multiferroic study. Since the discovery of multiferroic behaviors in perovskite  $\text{BiFeO}_3$  and  $\text{TbMnO}_3$  [2,3], a large number of multiferroic materials with different physical mechanisms have been found in the last decade [9-13]. Among them, the spin-induced multiferroics have received the most attention because the ferroelectricity is induced by magnetic structures so that a strong ME coupling would be expected [14-16]. Several theories such as spin-current model (or inverse Dzyaloshinskii-Moriya interaction), exchange striction mechanism and  $d-p$  hybridization mechanism have been proposed to account for the spin-induced ferroelectricity in ME multiferroics by special spin textures such as non-collinear spiral spin structures and collinear E-type antiferromagnetic (AFM) structure with zigzag spin chains [17-21]. It is well known that a cubic perovskite lattice is unfavorable for ferroelectricity due to the existence of an inversion center. However, the total symmetry for an ME multiferroics is the product of the crystal and magnetic symmetries. Therefore, in principle, it is possible to find an ME multiferroics in a cubic perovskite system if its magnetic structure breaks the space inversion symmetry. Nevertheless, such an intriguing case has never been found in previous studies.

The A-site ordered perovskite with a chemical formula of  $AA'_3B_4O_{12}$  provides an opportunity for searching ME multiferroics in a cubic lattice. This type of ordered perovskite can be formed when three quarters of the A-site of a simple  $ABO_3$  perovskite is substituted by a transition-metal ion  $A'$  (Fig. 1a) [22]. Since both  $A'$  and B sites accommodate magnetic transition-metal ions, multiple magnetic interactions may develop while the crystal structure can be finely tuned by selecting appropriate  $A'$  and B elements to maintain a cubic lattice [23-27]. In this letter, we report that the A-site ordered perovskite  $LaMn_3Cr_4O_{12}$  (LMCO) with cubic symmetry shows a spin-driven multiferroic phase with strong ME coupling effects. The unique multiferroic behavior in this cubic perovskite originates from a nontrivial effect involving the interactions between two magnetic sublattices. The present study thus not only provides the first example of multiferroics in a cubic perovskite system but also opens up new insights on the physical mechanisms of multiferroics.

The detailed experimental and calculation methods adopted in this work are described in the Supplementary Information [28]. The obtained LMCO was proved to crystallize in an A-site ordered perovskite structure with cubic symmetry of  $Im-3$  at room temperature (Fig. 1a) and exhibit two AFM transitions on cooling (Fig. 2a) [29]. Our neutron powder diffraction (NPD) data shown in Fig. 1b demonstrates that this cubic

structure persists down to 2 K, in agreement with the low-temperature X-ray diffraction (XRD) and Raman spectrum results (Supplementary Figs. S1 and S2 of [28], respectively). Meanwhile, based on the temperature dependence of the magnetic peaks (111) and (100) (Figs. 1c and 1d), the NPD results confirm that the spin orderings of Mn and Cr ions lead to the AFM transitions at  $T_{\text{Mn}} \sim 50$  K and  $T_{\text{Cr}} \sim 150$  K, respectively. Furthermore, the NPD refinements produce collinear G-type AFM spin structures for both of the A'-site Mn-sublattice and the B-site Cr-sublattice with the propagation vector of (111)/(100) for Cr/Mn-sublattice and the spin orientations most probably along the equivalent [111] direction (Figs. 1e-g and Supplementary Fig. S3 of [28]). This collinear AFM spin configuration is consistent with the linear magnetization behaviors observed at different temperatures (Supplementary Fig. S4 of [28]).

Figure 2a shows the temperature dependence of the dielectric constant  $\epsilon$  and magnetic susceptibility  $\chi$ . Corresponding to the AFM phase transition occurred at  $T_{\text{Mn}}$ , the  $\epsilon$  also experiences a sharp anomaly. Moreover, this dielectric variation is independent on frequency, implying possible ferroelectric phase transition coupled with the AFM ordering of Mn spins. The ME coupling thus may occur at the onset of  $T_{\text{Mn}}$  in the cubic perovskite LMCO. By comparison, another broadening and frequency-dependent dielectric anomaly is observed at about 110 K for

10 kHz and 155 K for 1 MHz. This relaxation behavior is reminiscent to a ferroelectric transition probably originated from local structure inhomogeneity and/or some extrinsic effects as will be discussed later [40].

These two ferroelectric phase transitions are further studied by measuring pyroelectric current ( $I_p$ ) to derive the ferroelectric polarization ( $P$ ) with both positive and negative electric ( $E$ ) poling procedures from 200 K down to 5 K, as shown in Figs. 2b and 2c. Obviously, the  $I_p$  and  $P$  are completely switchable by the poling  $E$  reversal. The most striking finding is that the Mn spin ordering transition is coupled with a sharp change in both  $I_p$  and  $P$  at  $T_{Mn}$  (Figs. 2b and c and the insets), strongly indicates that the presence of this low-temperature ferroelectric phase transition (FE1) is closely related to the magnetic ordering of Mn sublattice, in agreement with the dielectric constant measurements. In addition, at the high temperature region, the  $I_p$  and  $P$  are found to gradually emerge below about 180 K, and then a broad peak in  $I_p$  is formed near 125 K (Fig. 2b). Since these two characteristic temperatures (180 and 125 K) are different from the value of  $T_{Cr}$  (150 K), the associated ferroelectric phase (FE2) seems to be of non-magnetic origin.

We noticed that the drastic changes of  $I_p$  at  $T_{Mn}$  are not a single peak or dip but unusual dip-peak features and vice versa for +Poled and -Poled curves, respectively (inset of Fig. 2b). Accordingly, the obtained  $P(T)$

curves slightly decreases and then increases or vice versa for +Poled or -Poled on cooling around  $T_{\text{Mn}}$  (inset of Fig. 2c). It implies that there exist two independent polarizations superposed below  $T_{\text{Mn}}$ . To prove this point, we performed two different poling  $E$  schemes to pass either 180 K or  $T_{\text{Mn}}$  (= 50 K) only. In sharp contrast to the dip-peak features in  $I_p$  with poling  $E$  across both  $T_{\text{Mn}}$  and 180 K (200-5 K, +Poled in Fig. 2b and Supplementary Fig. S5b of [28]), only a single dip (200-75 K, +Poled) or peak (75-30 K, +Poled) in  $I_p$  was observed in each poling scheme, respectively, as shown in Fig. 3a and Supplementary Fig. S5a of [28]. Correspondingly, the obtained net polarization changes ( $\Delta P = P(T) - P(50 \text{ K})$ ), which represent the influence of Mn ordering to the  $P$  values, show negative values when  $E$  is applied only across 180 K, whereas positive  $\Delta P$  values are obtained with  $E$  applying only across  $T_{\text{Mn}}$  as shown in Fig. 3b (for details, see Supplementary Fig. S5c of [28]). The single dip in  $I_p$  (200-75 K, +Poled) means that, although the FE2 phase sets in at a temperature much higher than  $T_{\text{Mn}}$ , the spin ordering of Mn ions still causes a decrease of  $P$  in magnitude in this phase. More interesting, the peak in  $I_p$  (75-30 K and +Poled) reveals that the FE1 phase which develops at  $T_{\text{Mn}}$  is an independent ferroelectric phase from the FE2 phase. Since the FE1 phase strongly couples with the AFM ordering of Mn-sublattice, the present cubic perovskite LMCO can be regarded as a new spin-driven multiferroics below  $T_{\text{Mn}}$ .

To further confirm that the observed pyroelectric signals come from intrinsic ferroelectricity instead of the possible space charge effect, we applied different external magnetic fields to measure the pyroelectric and dielectric properties. Considerable anisotropic ME and magnetodielectric effects are found in these two FE phases at and below  $T_{Mn}$ . As shown in Fig. 3a, when an external magnetic field  $H//E$  is applied up to 12 T in the poling and measuring processes, the absolute values of  $I_p$  near  $T_{Mn}$  are enhanced by about one order in magnitude for both phases. The calculated  $|\Delta P|$  values in both FE phases also increase from  $\sim 15$  to  $\sim 68$   $\mu\text{C}/\text{m}^2$  at 30 K (Fig. 3b). In the  $H\perp E$  configuration, however, the  $I_p$  near  $T_{Mn}$  are found to be completely suppressed above 7 T field (not shown here). Similarly, the dielectric constant  $\epsilon$  also shows significantly changes under magnetic field at and below  $T_{Mn}$ . For  $H//E$  configuration, the sudden jump in  $\epsilon$  around  $T_{Mn}$  for  $\mu_0 H = 0$  changes into a sharp peak for  $\mu_0 H \geq 3$  T (Fig. 3c). By comparison, the  $H\perp E$  configuration remarkably decreases the dielectric jump at  $T_{Mn}$  so that almost no dielectric anomaly is observed with field above 7 T (Fig. 3d), in coherence with the complete suppression of electric polarization at this  $H$  and  $E$  configuration under high field mentioned above. On the other hand, however, with increasing magnetic field, there is not remarkable change in  $\epsilon$  above  $T_{Mn}$  either in  $H//E$  or  $H\perp E$  configuration, revealing different origins for FE1 and FE2 phases. Anyway, our magnetic-field dependent measurements show that

the FE1 phase has strong anisotropic  $H$  dependent behaviors, excluding extrinsic origin of space charge for this multiferroic phase. Moreover, the magnetoelastic-coupling induced  $I_p$ , which was misunderstood as the evidence of ferroelectricity in a centrosymmetric perovskite  $\text{SmFeO}_3$  [41-44], can also be ruled out in our LMCO (Supplementary Information [28]).

We now discuss possible mechanisms responsible for the low temperature Mn spin ordering induced ferroelectricity in the cubic perovskite LMCO. First, both the inverse Dzyaloshinskii-Moriya interaction and the spin-current model, which are related to the cross products of spins, are excluded due to the collinear spin configuration of LMCO (Figs. 1e-g). **The exchange striction mechanism induced electric polarization is related to the dot product of a pair of spins which is independent from the spin orientations if the two spins are always parallel or antiparallel with each other. In contrast, based on the magnetic point group analysis and theoretical calculations shown later, the polarization direction of FE1 phase is always simultaneously changed with the spin orientations (one of the equivalent [111] directions). It means that the exchange striction mechanism does not contribute to the polarization in FE1 phase if there is any.** As a consequence, these conventional ME mechanisms are invalid to explain the present ferroelectric behaviors.

We then try to resolve the issue by performing magnetic point group

analysis. In the temperature region of  $T_{\text{Mn}} < T < T_{\text{Cr}}$ , the Cr sublattice is ordered in a G-type AFM manner with spin orientation along [111] direction (Fig. 1e). Since the crystal space group is  $Im\bar{3}$ , the magnetic point group should be a non-polar  $\bar{3}'$  group with space inversion center. At  $T < T_{\text{Mn}}$ , the Mn sublattice is also ordered into a G-type AFM structure with non-polar  $\bar{3}$  group as its own magnetic point group (Fig. 1f). Therefore, no polarization can be induced by either Cr or Mn spin ordering alone. However, when we consider Mn and Cr sublattices together below  $T_{\text{Mn}}$ , the system magnetic point group is a polar group  $\bar{3}$  (Fig. 1g), which allows a polar along the spin direction. It suggests that the ferroelectric polarization of FE1 phase most probably arises from the Mn and Cr spin configurations together, ruling out any possibility of single spin mechanism, *e.g.*, the *d-p* hybridization model [20].

The density functional theory calculations have been performed to further understand the spin-driven ferroelectricity of FE1 phase (for details, see Supplementary Information [28]). The results show: 1) Without considering the spin-orbit coupling (SOC) of magnetic ions, the calculated ferroelectric polarization for the experimental magnetic ground state is exactly zero in the FE1 phase; 2) If the SOC is switched on with all spins pointing parallel or antiparallel to the [111] axis as the NPD study suggested, even the exact high-symmetric structure can induce a small but nonzero ferroelectric polarization  $\sim 3.4 \mu\text{C}/\text{m}^2$  along the [111]

direction. This result, without any contribution from ionic displacement, is the pure electronic polarization; 3) The direction of pure electronic polarization can be switched by rotating the magnetic axis. These results are convincing to exclude the possible contribution from the inaccuracy of ionic relaxation, supporting the intrinsic ferroelectricity caused by the spin ordering; 4) When the ionic positions are further relaxed with SOC enabled, which gives a total polarization up to  $\sim 7.5 \mu\text{C}/\text{m}^2$ , still along the [111] axis. Although this small value may be not very precise due to the inaccuracy of ionic displacements, the value is comparable in the order of magnitude with experimental observation at zero field ( $\sim 15 \mu\text{C}/\text{m}^2$ , see Fig. 3b), and also consistent with magnetic symmetry analysis that the ground state magnetic structure is polarized. Note that since the three conventional mechanisms for spin-driven ferroelectricity are forbidden in the present cubic perovskite system, other possible exotic mechanisms involving the relativistic exchange interactions only generate a moderate polarization.

As for the FE2 phase, since the pyroelectric current emerges above  $T_{\text{Cr}}$  and forms a broad peak at about 125 K, its origin is clearly not related to any spin ordering. Such a feature, on the one hand, may be ascribed to an extrinsic effect such as space charges trapped at the grain boundaries or possible defects as reported elsewhere [46,47]. On the other hand, we noticed that some  $\text{ABO}_3$  perovskites like  $\text{YCrO}_3$  and  $\text{SmCrO}_3$  with  $\text{Cr}^{3+}$

ions at the B site also displayed similar electric polarizations above the AFM temperatures [48,49]. Neutron pair distribution function (PDF) illustrated that this type of polarization originated from the “local non-centrosymmetric effect” caused by the local displacements of the second-order Jahn-Teller  $\text{Cr}^{3+}$  cations, whereas the macroscopic crystal structure was unchanged to be centrosymmetric. In the present LMCO, although the long-range crystal structure is stabilized down to 2 K, similar local displacements of  $\text{Cr}^{3+}$  cations are possible to occur, as implied by the relaxation behavior in dielectric constant in the high-temperature region (Fig. 2a) as well as the anomalies observed in Raman spectra around 180 K (see Supplementary Fig. S2 and related description in [28]). More experiments such as high-resolution neutron PDF are needed to reveal the exact origin of FE2 phase in the future.

Here, we would like to emphasize that the ME multiferroicity found in the present LMCO at the onset of about 50 K is quite unique among all the known multiferroic systems in that it occurs in a true cubic perovskite system with simple and collinear spin alignments. Due to the high symmetry in lattice and spin structures, the three major mechanisms to induce ferroelectric polarization by magnetic ordering fail to play roles. The present work therefore not only provides the first example of cubic perovskite multiferroics but also opens up a new arena to study the unexpected ME coupling mechanisms.

## **Acknowledgments**

We thank H. J. Xiang for useful discussion. This work was partly supported by 973 Project of the Ministry of Science and Technology of China (Grant No. 2014CB921500), the Strategic Priority Research Program of the Chinese Academy of Sciences (Grants No. XDB07030300, XDB07030200). Y. Chai, Y. Sun, H. Zhang and S. Dong were supported by the NSFC (Grant Nos. 11374347, 11227405 and 51322206). Research conducted at ORNL's High Flux Isotope Reactor was sponsored by the Scientific User Facilities Division, Office of Basic Energy Sciences, US Department of Energy.

X. Wang, Y. S. Chai and L. Zhou contributed equally to this work.

## **References:**

- [1] H. Schmid, *Ferroelectrics* **162**, 317 (1994).
- [2] J. Wang *et al.*, *Science* **299**, 1719 (2003).
- [3] T. Kimura, T. Goto, H. Shintani, K. Ishizaka, T. Arima, and Y. Tokura, *Nature* **426**, 55 (2003).
- [4] N. A. Spaldin and M. Fiebig, *Science* **309**, 391 (2005).
- [5] W. Eerenstein, N. D. Mathur, and J. F. Scott, *Nature* **442**, 759 (2006).
- [6] S.-W. Cheong and M. Mostovoy, *Nat. Mater.* **6**, 13 (2007).
- [7] R. Ramesh and N.A. Spaldin, *Nat. Mater.* **6**, 21 (2007).
- [8] K. F. Wang, J. M. Liu, and Z. F. Ren, *Adv. Phys.* **58**, 321(2009).

- [9] Y. Tokura, S. Seki, and N. Nagaosa, Rep. Prog. Phys. **77**, 076501 (2014).
- [10] J. F. Scott, NPG Asia Mater. **5**, e72 (2013).
- [11] J. Ma, J. M. Hu, Z. Li, and C. W. Nan, Adv. Mater. **23**, 1062 (2011).
- [12] B. Van Aken, T. T. M. Palstra, A. Filippetti, and N. A. Spaldin, Nat. Mater. **3**, 164 (2004).
- [13] N. Ikeda *et al.*, Nature **436**, 1136 (2006).
- [14] L. C. Chapon, P. G. Radaelli, G. R. Blake, S. Park, and S.-W. Cheong, Phys. Rev. Lett. **96**, 097601 (2006).
- [15] T. Goto, G. Lawes, A. P. Ramirez, and Y. Tokura, Phys. Rev. Lett. **92**, 257201 (2004).
- [16] T. Kimura, G. Lawes, and A. P. Ramirez, Phys. Rev. Lett. **94**, 137201 (2005).
- [17] H. Katsura, N. Nagaosa, and V. Balatsky, Phys. Rev. Lett. **95**, 057205 (2005).
- [18] I. A. Sergienko and E. Dagotto, Phys. Rev. B **73**, 094434 (2006).
- [19] I. A. Sergienko, C. Şen, and E. Dagotto, Phys. Rev. Lett. **97**, 227204 (2006).
- [20] T. Arima, J. Phys. Soc. Jpn. **76**, 073702 (2007).
- [21] M. Mostovoy, Phys. Rev. Lett. **96**, 067601 (2006).
- [22] Y. Shimakawa, Inorg. Chem. **47**, 8562 (2008).
- [23] Y. W. Long, N. Hayashi, T. Saito, M. Azuma, S. Muranaka, and Y.

- Shimakawa, Nature **458**, 60 (2009).
- [24] A. Prodi *et al.*, Nat. Mater. **3**, 48 (2004).
- [25] Z. Zeng, M. Greenblatt, M. A. Subramanian, and M. Croft, Phys. Rev. Lett. **82**, 3164 (1999).
- [26] R. D. Johnson, L. C. Chapon, D. D. Khalyavin, P. Manuel, P. G. Radaelli, and C. Martin, Phys. Rev. Lett. **108**, 067201 (2012).
- [27] G. Zhang *et al.*, Phys. Rev. B **84**, 174413 (2011).
- [28] See Supplemental Material for detailed experimental and calculation methods, related data and discussion, which includes Refs. [29-39, 41-45].
- [29] Y. W. Long, T. Saito, M. Mizumaki, A. Agui, and Y. Shimakawa, J. Am. Chem. Soc. **131**, 16244 (2009).
- [30] J. Rodriguez-Carvajal, Physica B **192**, 55 (1993).
- [31] P. E. Blöchl, O. Jepsen, and O. K. Andersen, Phys. Rev. B **49**, 16223 (1994).
- [32] G. Kresse and J. Hafner, Phys. Rev. B **47**, 558 (1993).
- [33] G. Kresse and J. Furthmüller, Phys. Rev. B **54**, 11169 (1996).
- [34] S. L. Dudarev, G. A. Botton, S. Y. Savrasov, C. J. Humphreys, and A. P. Sutton, Phys. Rev. B **57**, 1505 (1998).
- [35] S. Lv, H. Li, X. Liu, and J. Meng, J. Appl. Phys. **110**, 023711 (2011).
- [36] R. L. Johnson-Wilke *et al.*, Phys. Rev. B **88**, 174101 (2013).
- [37] A. Iyama and T. Kimura, Phys. Rev. B **87**, 180408(R) (2013).

- [38] N. Mufti *et al.*, J. Phys.: Condens. Matter **22**, 075902 (2010).
- [39] R. D. King-Smith and D. Vanderbilt, Phys. Rev. B **47**, 1651 (1993).
- [40] A. A. Bokov, and Z. G. Ye, J. Mater. Sci. **41**, 31 (2006).
- [41] J.-H. Lee, Y. K. Jeong, J. H. Park, M.-A. Oak, H. M. Jang, J. Y. Son, and J. F. Scott, Phys. Rev. Lett. **107**, 117201 (2011).
- [42] R. D. Johnson, N. Terada, and P. G. Radaelli, Phys. Rev. Lett. **108**, 219701 (2012).
- [43] C.-Y. Kuo *et al.*, Phys. Rev. Lett. **113**, 217203 (2014).
- [44] R. D. Johnson, K. Cao, F. Giustino, and P. G. Radaelli, Phys. Rev. B **90**, 045129 (2014).
- [45] N. Kolev *et al.*, Phys. Rev. B **66**, 132102 (2002).
- [46] J. F. Scott, J. Phys.: Condens. Matter **20**, 021001(2008).
- [47] K. Okazaki and H. Maiwa, Jpn. J. Appl. Phys. **31**, 3113 (1992).
- [48] K. Ramesha, A. Llobet, Th. Proffen, C. R. Serrao, and C. N. R. Rao, J. Phys.: Condens. Matter **19**, 102202 (2007).
- [49] M. Amrani, M. Zaghrioui, V. Phuoc, F. Gervais, and N. E. Massa, J. Magn. Mater. **361**, 1 (2014).

**Figure Captions:**

**FIG. 1.** (a) Schematics of crystal structure of LMCO with space group  $Im-3$ . (b) NPD patterns at selected temperatures. The indexed (111) and (100) peaks arise from the AFM ordering of the B-site Cr-sublattice and the A'-site Mn-sublattice, respectively. (c),(d) Temperature dependence of the integrated NPD intensities of (111) and (100) peaks, respectively. (e),(f) G-type AFM structure of the B-site Cr-sublattice and the A'-site Mn-sublattice with spin orientation along [111] direction, respectively. (g) A complete set of spin alignment composed of Cr and Mn spins below  $T_{Mn}$ . For clarity, La and O atoms are omitted in the structures. Blue ball: Cr atom; red ball: Mn atom.

**FIG. 2.** Temperature dependence of (a) dielectric constant  $\epsilon$  and magnetic susceptibility  $\chi$ , (b) pyroelectric current  $I_p$  and (c) ferroelectric polarization  $P$  in both +Poled and -Poled conditions. The  $\epsilon$  and  $I_p$  were measured without magnetic field. The insets of (b) and (c) show the enlarged views near 50 K.

**FIG. 3.** (a) Temperature dependence of  $I_p$  and (b) the difference of polarization  $\Delta P$  at different poling conditions and different magnetic fields below 50 K. (c),(d) Temperature dependence of  $\epsilon$  measured at 1 MHz and different magnetic fields with  $H//E$  and  $H\perp E$  configurations, respectively. The data have been shifted for clarity.

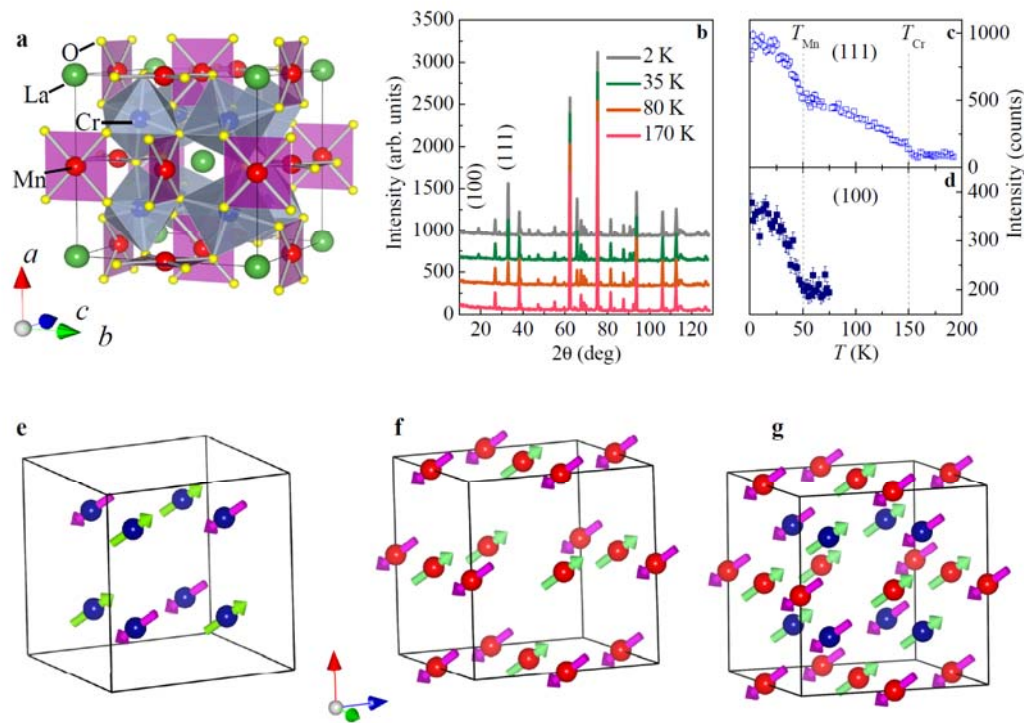


Figure 1

Xiao Wang *et al*

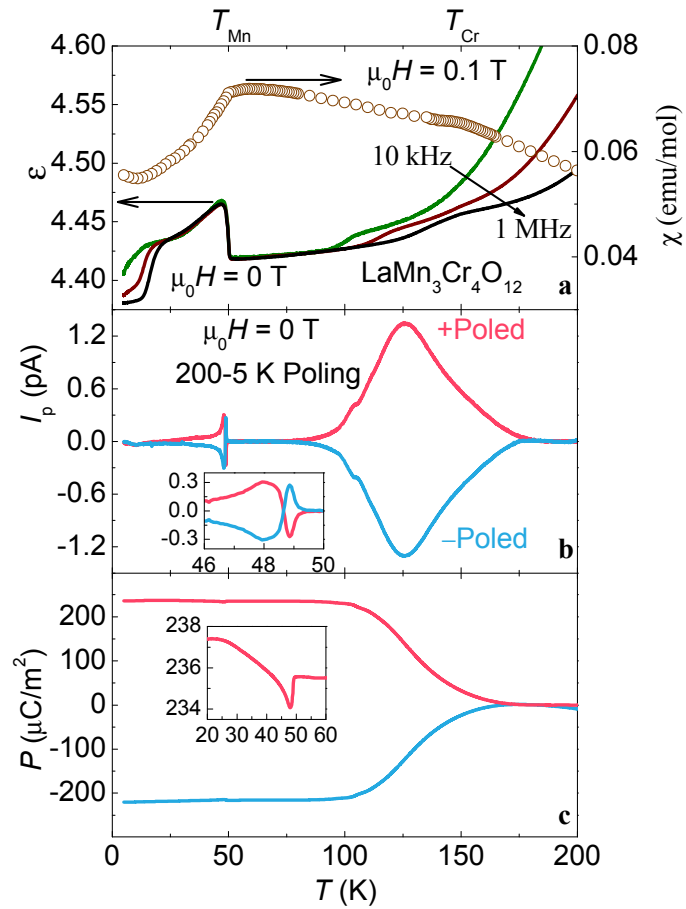


Figure 2

Xiao Wang *et al*

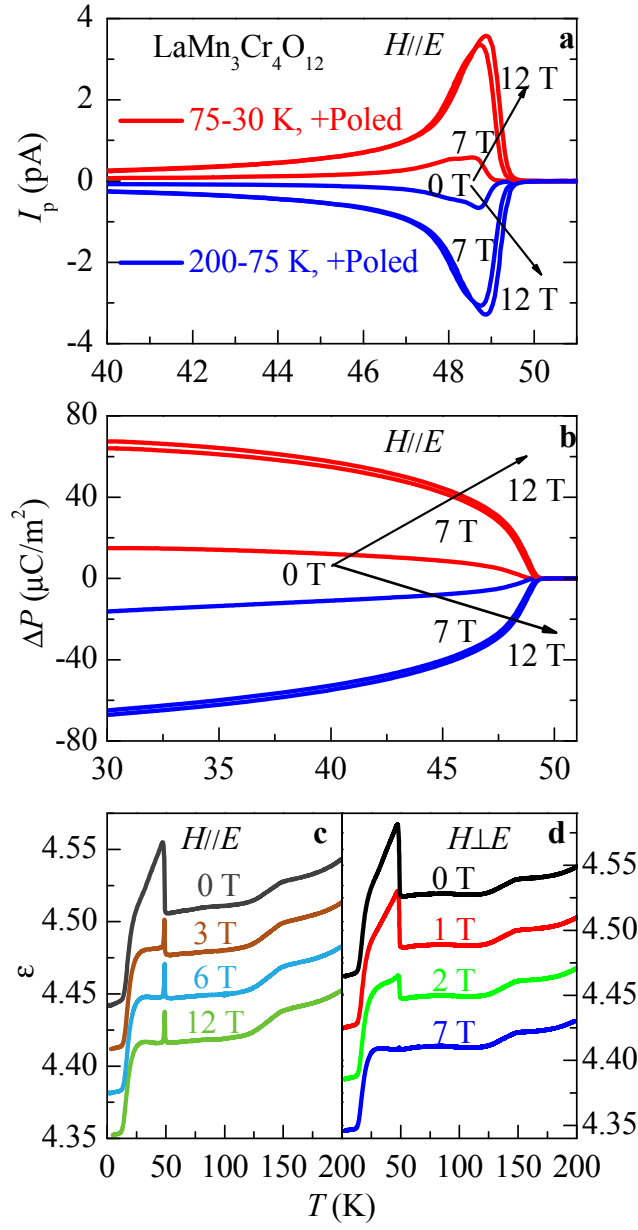


Figure 3

Xiao Wang *et al*